Royal Netherlands Meteorological Institute
Ministry of Infrastructure and the Environment

The EUMETSAT Network of Satellite Application Facilities

OSI SAF
Ocean and Sea Ice

EUMETSAT

Ocean and Sea Ice SAF

Technical Report
SAF/OSI/CDOP2/KNMI/TEC/RP/211

Analysis of ASCAT-B Transponder Calibration for Wind Processing

Jeroen Verspeek
Ad Stoffelen
Anton Verhoef

2013-10-16

Summary

The EUMETSAT transponder calibration effectively results in new ASCAT-B instrument gain values at each Wind Vector Cell (WVC) for each of the fore, mid and aft beams. In this report we describe and evaluate level 1b (L1b) corrections to the operational L1b ASCAT backscatter data version 901 (relative to 801) as provided by EUMETSAT based on their three transponder calibration campaign. Based on the OSI SAF cone visualisation tools at KNMI and the NWP Ocean Calibration (NOC) procedure, calibration of the ASCAT-B scatterometer is checked. Indeed, after reverse corrections the ASCAT wind product based on L1b version 901 shows very similar characteristics to the ASCAT scatterometer wind product based on L1b version 801 and meets the wind product requirements.

The operational OSI SAF Metop-B ASCAT level 2 wind product streams run at KNMI, using the validated ASCAT level 1b stream at full resolution and 25 km sampling as input, may be maintained without any significant effects on product quality. The new (901) L1b σ^0 stream will be corrected using the new linear scaling factors in the transformed z domain, which correspond to addition factors in the logarithmic domain (dB). These changes correspond to slightly resetting the ASCAT instrument gain per beam and per Wind Vector Cell (WVC) in order to maintain backscatter data consistency and wind product quality for the L1b processing versions 801 and 901.

Contents

Summary 2
Contents 3
1 Introduction 4
2 NOC correction 5
3 Normalisation correction 8
4 Shift in geolocation 10
5 Total NOC correction factors 12
6 NWP backscatter comparison 16
7 Wind statistics 17
7.1 Collocated wind statistics 19
8 MLE statistics and QC 20
9 Conclusions 24
Acronyms and abbreviations 26
References 27

1 Introduction

The Advanced Scatterometer (ASCAT) [Figa et al 2002] is part of the payload of the MetOp satellite series of which the first one, MetOp-A, has been successfully launched on October 19th, 2006 and the second one, MetOp-B on September 17th, 2012. ASCAT is a fan beam scatterometer with six fan beam antennae providing a swath of WVCs both to the left and right of the sub-satellite track. Each swath is thus illuminated by three beams and is divided into 41 WVCs of 12.5 km size, numbered from 1-82 from left to right across both swaths (when looking into the satellite propagation direction. EUMETSAT has provided the following level 1b datasets during the MetOp-B life time:

1) from 2012-09-17 (launch date) until 2013-06-24: version 8.01;
2) from 2013-06-24 onwards: version 9.01;

This report verifies a seamless transition in wind processing from version 801 to 901.

An operational OSI SAF ASCAT level 2 wind product stream is running at KNMI using the ASCAT L1b stream at 25 km sampling as input. The 12.5-km sampling coastal product is made from the ASCAT full resolution stream as input. The L1b σ^0 stream is corrected using linear scaling factors in the transformed z domain [Stoffelen and Anderson 1997], corresponding to addition factors in the logarithmic domain (dB). These changes correspond to resetting the ASCAT instrument gain per beam and per Wind Vector Cell (WVC). The objective is set to produce wind distributions similar to those from moored buoys and NWP models, using a Geophysical Model Function (GMF) that relates wind, incidence and azimuth angles to backscatter information. The GMF implies relative consistency between the different beams at the same incidence angles and the moored buoys provide an absolute calibration standard. Moreover, this methodology provides a transfer standard from the European Remote-sensing Satellite (ERS) scatterometer to the ASCAT era. The method is also applied to other scatterometers operating in the Ku-band.

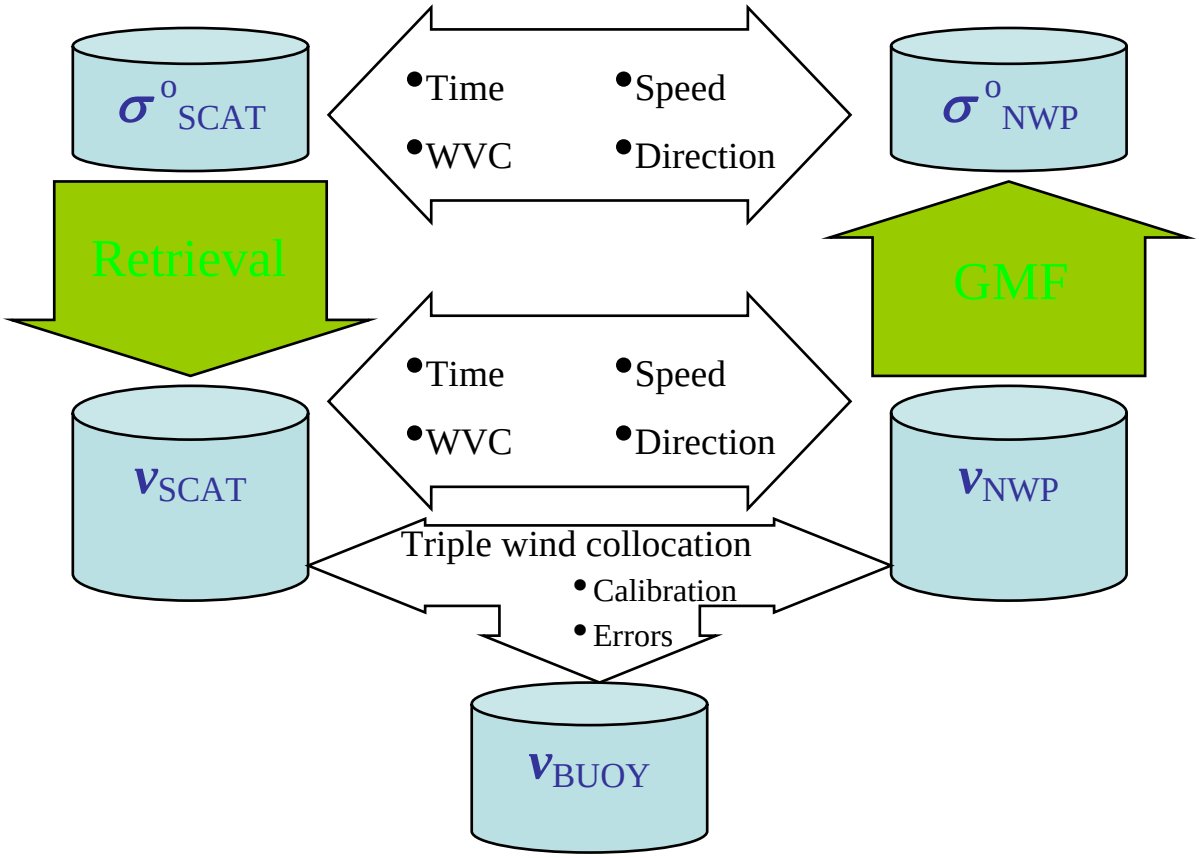

Figure 1 – Schematic depiction of the consistent calibration and validation methodology of scatterometer backscatter and wind information as applied for all scatterometers.

[Stoffelen and Anderson 1997] describe the so-called measurement space. In this space the three backscatter measurements are plotted along three axis, spanning the fore, mid and aft beam backscatter measurements. As the satellite propagates and the wind conditions on the ocean surface vary in each numbered WVC, the 3D measurement space will be filled. CMOD5 [Hersbach 2007] describes the geophysical dependency of the backscatter measurements on the WVC-mean wind vector as derived from ERS scatterometer data. Since this dependency involved two geophysical parameters, namely two orthogonal wind components (or wind speed and direction), the 3D measurement space is filled with measurements closely following a 2D surface [Stoffelen and Anderson 1997]. This folded surface is conical and consists of two sheets, one sheet for when the wind vector blows against the mid beam pointing direction (upwind section) and one for an along mid beam pointing direction wind vector (downwind section). The knowledge on the position of this surface through the Geophysical Model Function (GMF), CMOD5 provides a powerful diagnostic capability for the calibration and validation of the ASCAT scatterometer, since the same geophysical dependency should apply for both the ERS and MetOp scatterometers; see also [Anderson 2012].

Besides ocean calibration EUMETSAT relies on the rain forest response, the backscatter over sea ice and transponder measurements for ASCAT calibration [FIGA et al 2004]. In this report we explore ocean calibration to achieve a continuous quality for the ASCAT-B wind processing. We assume that the main challenge lies in setting the antenna pattern or gain settings of the six beams and explore normalisation corrections to the experimental L1b backscatter data as provided by EUMETSAT during the commissioning phase of MetOp by investigating a parallel stream of backscatter data provided bt EUMETSAT. A synchronized data set containing L1b version 801 and 901 was provided by EUMETSAT, ranging from 2013-05-30 to 2013-06-03. In this document this synchronized data set is used.

The L1B software identifier is written in the BUFR message and is used for automatic determination of the applicable correction table in the ASCAT Wind Data Processor (AWDP).

In section 2 and 3 the correction based on the NWP Ocean Calibration (NOC) residuals and the normalisation correction based on the averaged backscatter difference between the two level 1b software versions 901 and 801 are described respectively. Section 4 discusses the shift in geolocation between the two versions. Section 5 shows the data in measurement space as well as the total (NOC+normalisation) correction factors. In sections 6, 7 and 8 the ocean calibration results, the wind statistics, and the Maximum Likelihood Estimator (MLE) statistics are discussed, respectively. The conclusions and outlook are presented in section 9.

2 NOC correction

The NWP Ocean Calibration (NOC) method resides in direct comparison of measured σ_0 data with simulated values from NWP winds using the GMF [Stoffelen, 1998; Freilich, 1999; Verspeek, 2011]. For the ASCAT and ERS scatterometers, the NOC estimates <z>, i.e. the mean transformed backscatter over the ocean for a uniform wind direction distribution and compares it with the mean measured backscatter over the ocean for a given wind distribution.

The NOC technique [Stoffelen 1998] is used to assess the difference between scatterometer backscatter data and simulated backscatter data out of collocated NWP winds using the GMF. Discrepancies between mean measured and simulated backscatter may be due to instrument calibration, systematic and random errors in NWP wind speed and direction and GMF errors. These sources of error should therefore be analyzed carefully. The NOC method is based on the analysis of a large measurement dataset to estimate Fourier coefficients that can be directly compared to those in the CMOD5.N GMF. For any particular WVC in any beam the incidence angle is almost constant over the orbit and we can model the backscatter with

$$\sigma_0(v,\phi) = B_0(v)[1 + B_1(v)\cos\phi + B_2(v)\cos(2\phi)]^{1.6}$$

where v is wind speed and ϕ is wind direction with respect to the beam pointing direction. The mean backscatter is essentially determined by the value of B_0 with contributions from B_1 and B_2. In z-space, where $z = \sigma_0^{0.625}$, this becomes

$$z(v,\phi) = \frac{1}{2}a_0(v) + a_1(v)\cos\phi + a_2(v)\cos(2\phi)$$

where $a_0 = 2B_0^{0.625}$, $a_1 = B_1B_0^{0.625}$ and $a_2 = B_2B_0^{0.625}$. Integrating uniformly over the azimuth angle gives

$$\frac{1}{2\pi}\int_0^{2\pi} z(v,\phi)\,d\phi = \frac{1}{2}a_0(v)$$

As such, when the wind direction distribution is sampled uniformly for all wind speeds, the mean of $2a_0$ should be identical to the mean of z. This means that uncertainties in a_1 and a_2 do not contribute to the error in the simulated mean z.

To arrange for a uniform wind direction distribution, we split the data into wind speed bins and azimuth angle bins. Bins are defined so that they are large enough to contain a certain minimum number of measurements and small enough to provide a good approximation of the integral. In the following, indices i and j refer to wind speed bin i and azimuth angle bin j respectively. Index k is used to refer to an individual measurement z_k. Parameters I, J and K refer to the total number of bins or measurements, so $i=1, 2 \ldots, I$, $j=1, 2 \ldots, J$ and $k=1, 2 \ldots, K(i,j)$.

The mean z in a fixed wind speed row is $z(i)$:

$$z(i) = \frac{1}{J}\sum_{j=1}^{J}\frac{1}{K(i,j)}\sum_{k=1}^{K(i,j)} z_k(i,j)$$

Summation over the wind speed rows gives

$$\langle z\rangle = \frac{1}{KJI}\sum_{i=1}^{I} KJ(i)z(i)$$

with

$$KJ(i) = \sum_{j=1}^{J} K(i,j), \quad KJI = \sum_{i=1}^{I}\sum_{j=1}^{J} K(i,j)$$

<z> is the mean backscatter value over a uniform wind direction distribution and may be either measured or simulated by collocated NWP wind inputs and the GMF, where mainly the term as given by $a_0(v)$ or $B_0(v)$ contributes. Any discrepancy between the simulated and measured mean backscatter values is computed as a ratio. A ratio not equal to one may be related to inaccuracies in the instrument gain, e.g., beam pattern determination, or to errors in the NWP input winds and GMF.

This method needs only a few days of collocated ASCAT data and ECMWF winds to produce a reasonable estimate of difference in a_0. We use CMOD5.N with the ECMWF equivalent neutral 10-meter winds to calculate model backscatter values corresponding to the collocated measured

values and apply the process as described above. The difference between the two values of a_0 then provides an estimate of the mean difference between model and measurement backscatter.

The ocean calibration gives residuals in backscatter as a function of incidence angle for each antenna. When these residuals are stable over time they may be used as correction factors for errors in the instrument, for monitoring instrument health or for GMF development.

The consistency of the backscatter measurements as measured by fore, mid and aft beam may be visualised before and after NOC. We use the OSI SAF visualisation package [Verspeek 2006-2] to produce visualisation plots in z-space, i.e., (z_{fore}, z_{aft}, z_{mid}) where $z=(\sigma^\circ)^{0.625}$ [Stoffelen, 1998]. Figure 2 is an example of such a visualisation from ASCAT. The double cone surface of CMOD5.N is depicted in blue. The measured data is shown as a cloud of black points around the cone surface. The cloud of ASCAT backscatter (σ°) triplets (corresponding to the fore, mid, and aft beams) match the CMOD5.N GMF in the 3-D measurement space [Hersbach 2007].

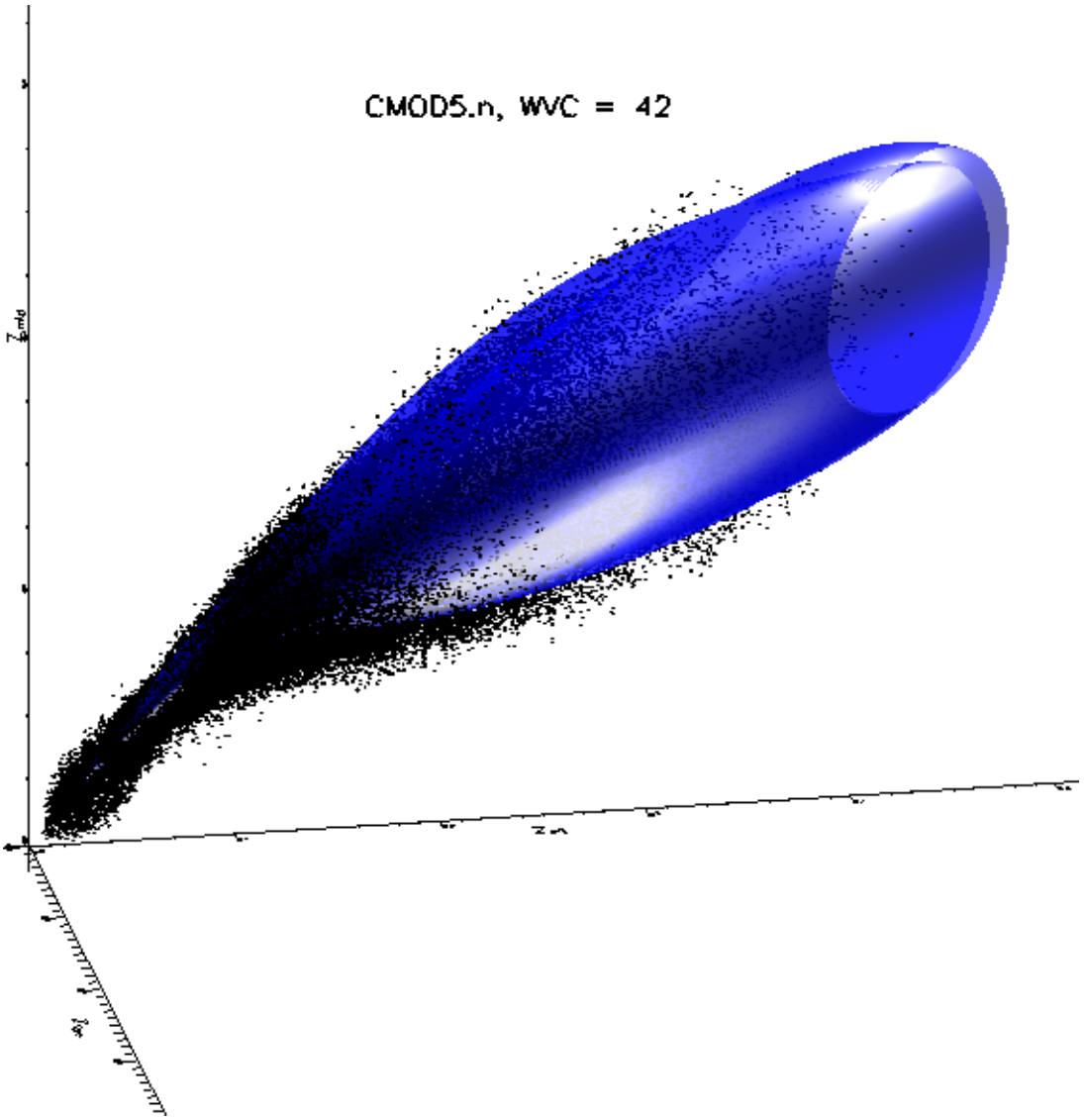

Figure 2 – CMOD5.N wind cone with measured data points for WVC 42, the innermost WVC of the right swath.

3 Normalisation correction

The NOC corrections were applied to adapt the backscatter values in the original version 801 L1b stream [Verspeek, Verhoef and Stoffelen 2013]. However, since the launch of METOP-B, EUMETSAT carried out a transponder calibration campaign and their L1B processing evolved from version 801 to 901. Here we describe the method used to compute and "reverse engineer" the backscatter calibration change. A correction that accounts for differences in the level 1B software processing versions is computed and subsequently applied. These corrections are able to transform the ASCAT backscatter measurements from each L1b calibration cycle to the next cycle within a few hundredths of a dB with L1b software version 801 taken as the reference. Thus the results are made independent of the L1b software version that is used. This method has also been applied for ASCAT-A [Verspeek et al 2011].
The normalisation factors are assumed to be multiplication factors in linear space as for NOC. Because all correction factors are linear, the corrections can be applied on top of each other. Normalisation correction tables are determined for each update of the L1b data. This is done by averaging the σ^0 differences in dB value from the new L1b data stream and the parallel original L1b data steam over one or more collocated orbits. The differences appear rather constant and show insignificant spread, confirming that the main effect in these conversions is a gain factor. Figure 3a) shows the average value per antenna and WVC of the difference in σ^0 value between the level 1b version 901 and 801 data stream. Figure 3b) shows the standard deviation (SD) for the corrections shown in Figure 3a). Figure 3c) and Figure 3d) show the same for the 25 km resolution product. Synchronized batches are used for an assessment of the spread in the differences (SD). The differences show a smooth course. The SD plot in Figure 3b) shows an enhanced level for the left fore and right aft beam SD.

The reason for the high backscatter SD between current and new calibrations for these beams is the introduction of the de-pointing angles from the first ASCAT-B transponder calibration. The current (version 801) calibration was based on a rough collocation analysis between ASCAT-A and ASCAT–B and could not provide the ASCAT-B de-pointing angles with any meaningful precision, so they were set to zero to start with. After the transponder calibration, those have been determined and introduced in the processing with the new calibration (version 901). The effect of this is a slight change in the geolocation (and geometry) of the full resolution backscatter values which is especially pronounced for the left fore and right aft beams. Thus the higher SD values for these beams are to be expected due to the natural variability in surface backscatter. In line with this, the relative changes for these two beams are largest at the smallest scale: 12.5 km.

For the other beams the SD shows small values indicating that the pattern is persistent. It is an order of magnitude below the typical calibration changes. This is comparable with earlier ASCAT-A calibration changes, thus guaranteeing a constant-quality backscatter input to the L2 processing.

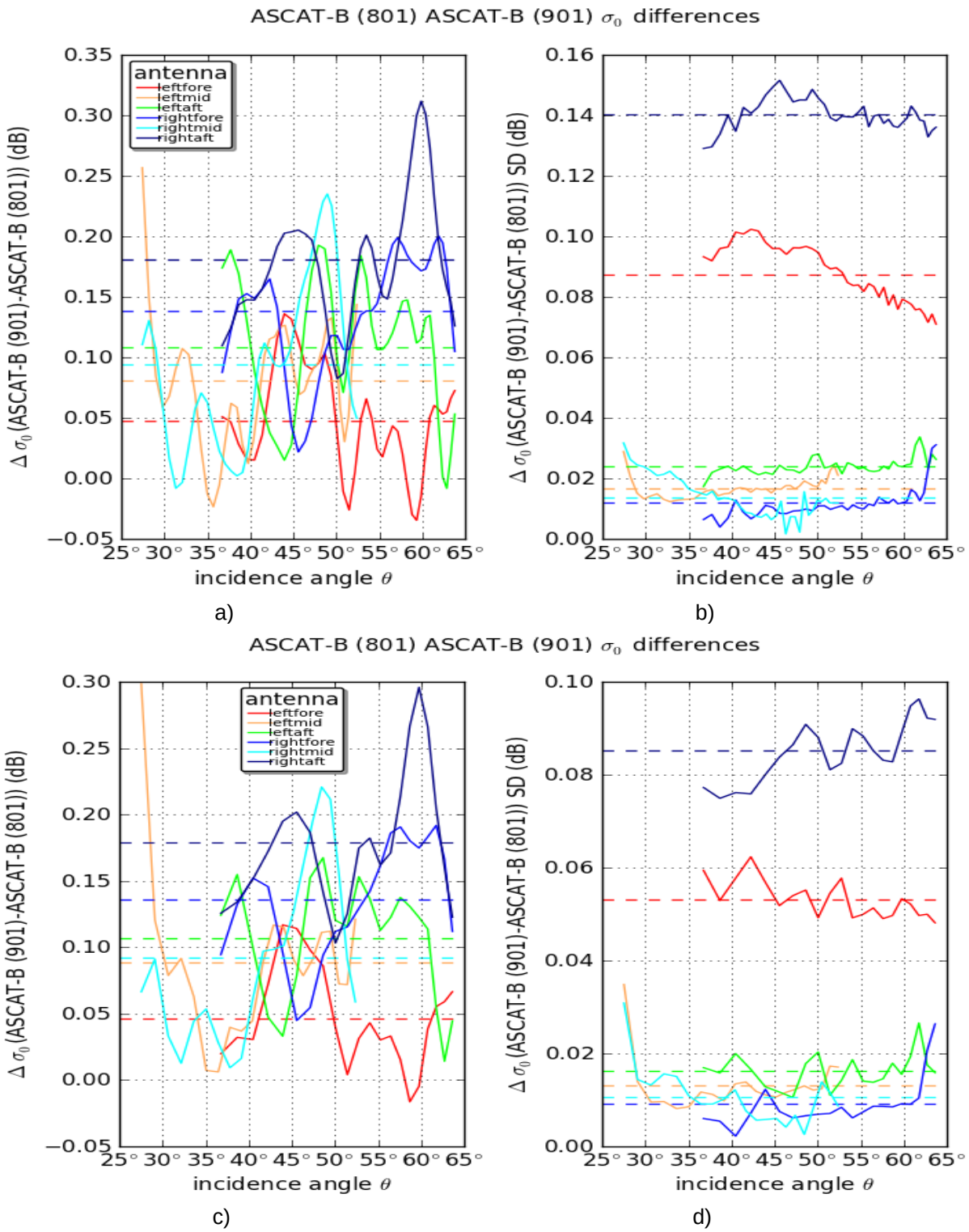

Figure 3 – Average and standard deviation of the difference between the L1b versions 901 and 801 for the fore, mid and aft antenna as a function of incidence angle.
a) average of σ^0 difference, 12.5 km resolution
b) standard deviation of the difference, 12.5 km resolution
c) average of σ^0 difference, 25 km resolution
d) standard deviation of the difference, 25 km resolution

Figure 4a) and Figure 4c) show the backscatter differences from the right fore and right aft antennas respectively on a map of West-Africa from data of 2013-05-30. Any dependency of the difference in backscatter on geographical location should be visible in these figures. The

dependency appears to be mainly on WVC number or incidence angle. The orbits have a systematic pattern across the swath, showing the WVC dependency of the correction. Figure 4b) and Figure 4d) show the same data corrected for the average L1b 901-801 σ^0 difference from Figure 3a). The remaining differences are very small and rather uniform, no pattern as function of incidence angle can be observed.

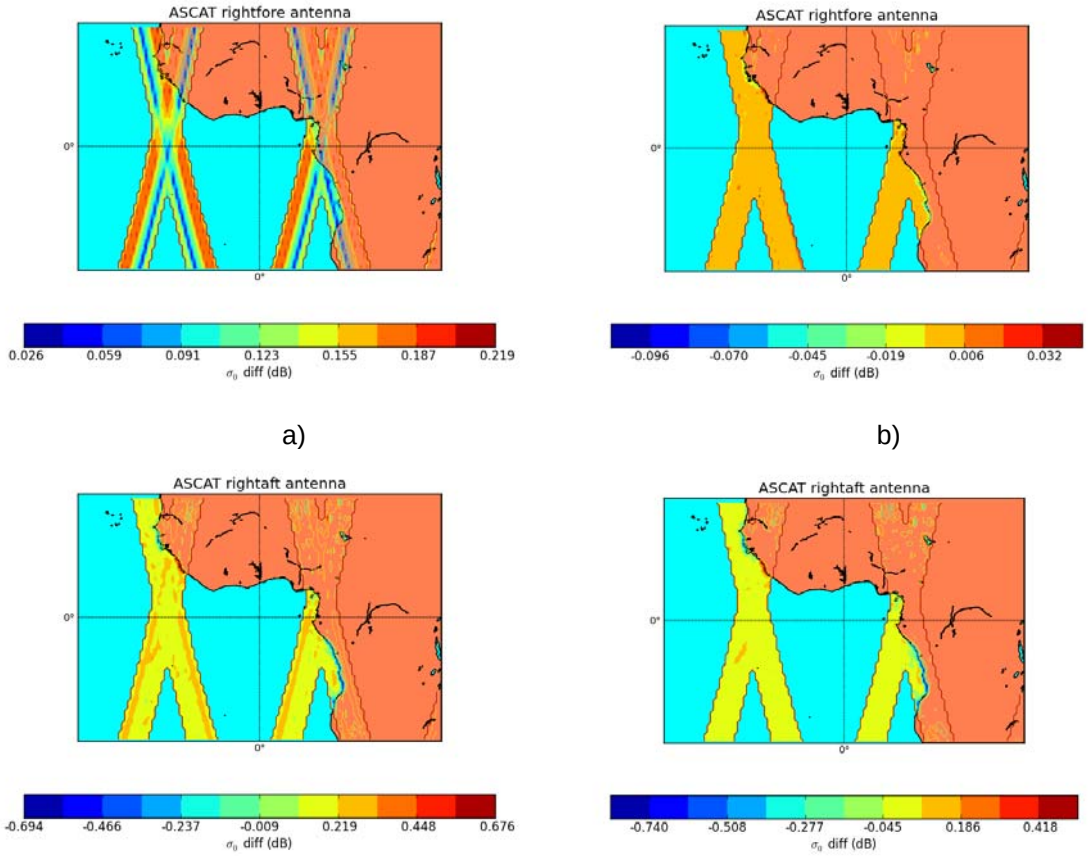

Figure 4 – Spatial plot (West-Africa) of the average difference in σ^0 of the L1b 901-L1b 801 data for the right fore and right aft antenna . 12.5 km resolution data from 2013-05-30 to 2013-06-03 are used.
a) right fore antenna
b) right fore antenna, correction for L1b differences applied
c) right aft antenna
d) right aft antenna, correction for L1b differences applied

4 Shift in geolocation

As mentioned in section 3 the enhanced level for the left fore and right aft beam SD in Figure 3b) is caused by a slight change in the geolocation (and geometry) of the full resolution backscatter values. This effect will be most pronounced for high resolutions in combination with steep changes in backscatter, as is typically the case near the coast.

Figure 5 shows the full resolution product near the West-African coast for a) version 8.01 and b) version 9.01. There is a small shift in location of the swath which is not visible by eye from these figures, but it can be observed when the two images are toggled. The full-resolution product forms the basis for all gridded level 1b backscatter products.

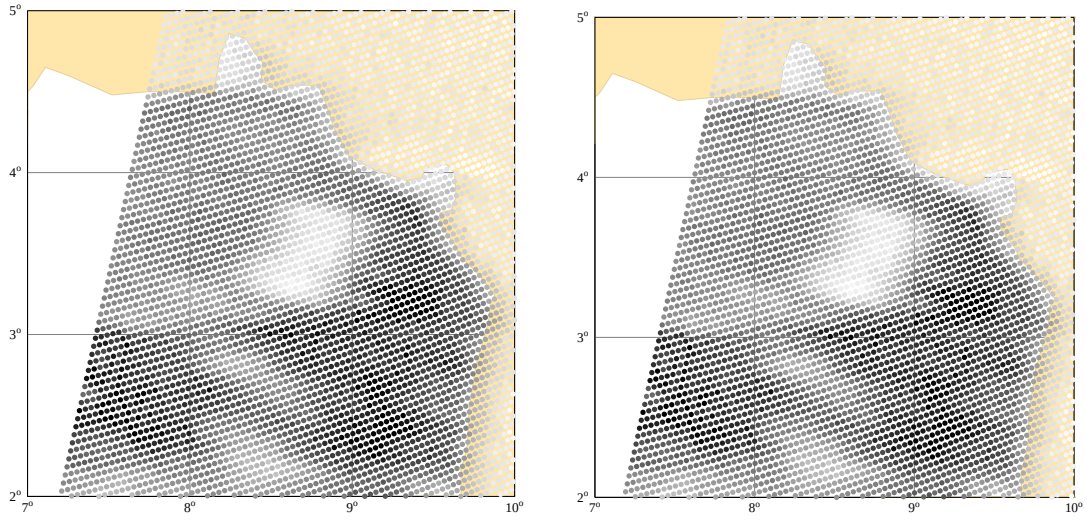

a) b)

Figure 5 - Full-resolution product near the West-African coast for a) version 8.01 (SZF_O) and b) version 9.01 (SZF_C).The two versions are shifted by a small distance of ~1 km with respect to each other. The backscatter scale is from -40 dB (black) to -7 dB (white).

Figure 6 shows the backscatter difference between the gridded 12.5 km Hamming window filtered products from version 9.01 and 8.01. Figure 6a) shows the rightaft antenna backscatter difference for a descending path and Figure 6b) for an ascending path. As can be seen the difference is small everywhere expect near land-sea (sea-land) transitions. Here the steep variation in σ^0 causes larger differences. The differences are the largest in the across-track direction. The sign of the difference is depending on whether the transition is sea-land or land-sea, when looking across-track in the direction of increasing incidence angle. The differences are present for all antennas (not shown) but are the largest for the leftfore and rightaft antenna. This is the cause of the larger SD in Figure 3b) for these antennas.

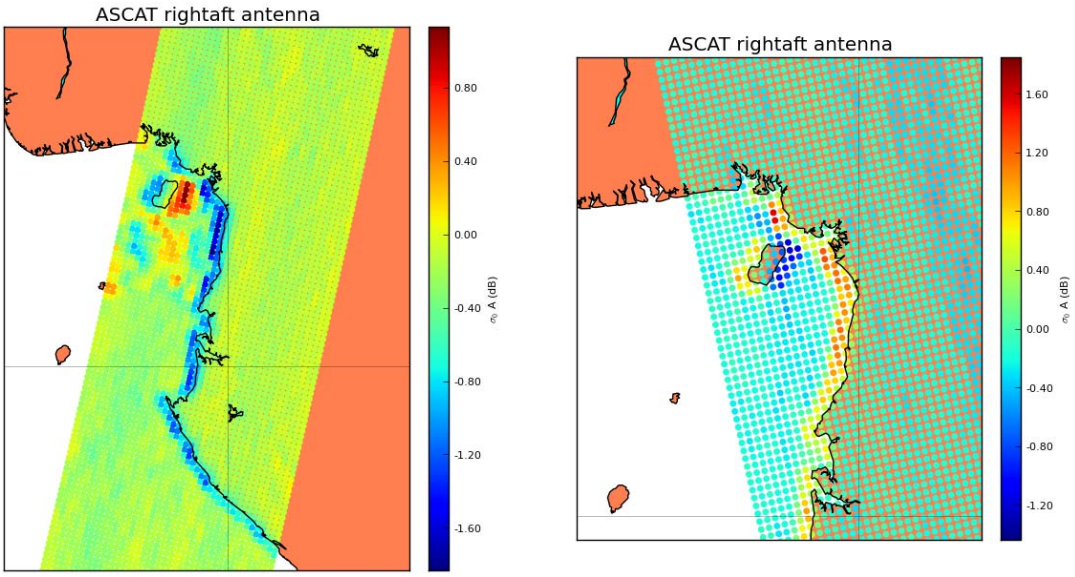

a) b)

Figure 6 – Backscatter difference (version 9.01-version 8.01) for the 12.5 km WVC product with Hamming window filtering for the rightaft antenna. a) descending track and b) ascending track

On overall wind statistics these coastal effects are small because the fraction of coastal WVCs with valid wind is small compared to all WVCs with valid wind. Coastal points are more sensitive to errors in geolocation but the shift in geolocation as present in Figure 5 is only very small. So the effect on e.g. the coastal product will be small too.

5 Total NOC correction factors

A total correction is applied to adapt the backscatter values in the L1b stream version 901, which consists of the NOC correction and the normalization correction as discussed in sections 2 and 3. The correction factors are again determined per wind vector cell (WVC) and beam. In the following sections GMF version CMOD5.N is used in the ASCAT Wind Data Processor (AWDP) and the ocean calibration. CMOD5.N is a version of CMOD5 that is adapted for equivalent neutral winds. The shape of the wind cone for CMOD5 and CMOD5.N is identical. The 28 fit-coefficients in the CMOD function have been recalculated for CMOD5.N by ECMWF, which lead to negligible deviations within the numerical precision of the fit procedure. The equivalent neutral wind speed GMF is the result of a triple collocation study with ECMWF winds and buoy winds [Portabella and Stoffelen 2009].

Figure 7 shows CMOD5.N and the corrected L1b version 901 data for the plane $z_{fore} = z_{aft}$. Figure 8 shows the same as Figure 7 but now for the projection of the wind cone and data points on the plane $z_{mid} = 0$. Figure 9 shows the intersection of the cone with the plane $z_{fore} + z_{aft} = 2z_{ref}$, for several values of z_{ref}, which correspond to (approximately) constant wind speed values. Also here the match between measurements and GMF is good. For other WVCs similar plots have been examined (not shown). For all examined WVCs the correspondence between data and model appears good.

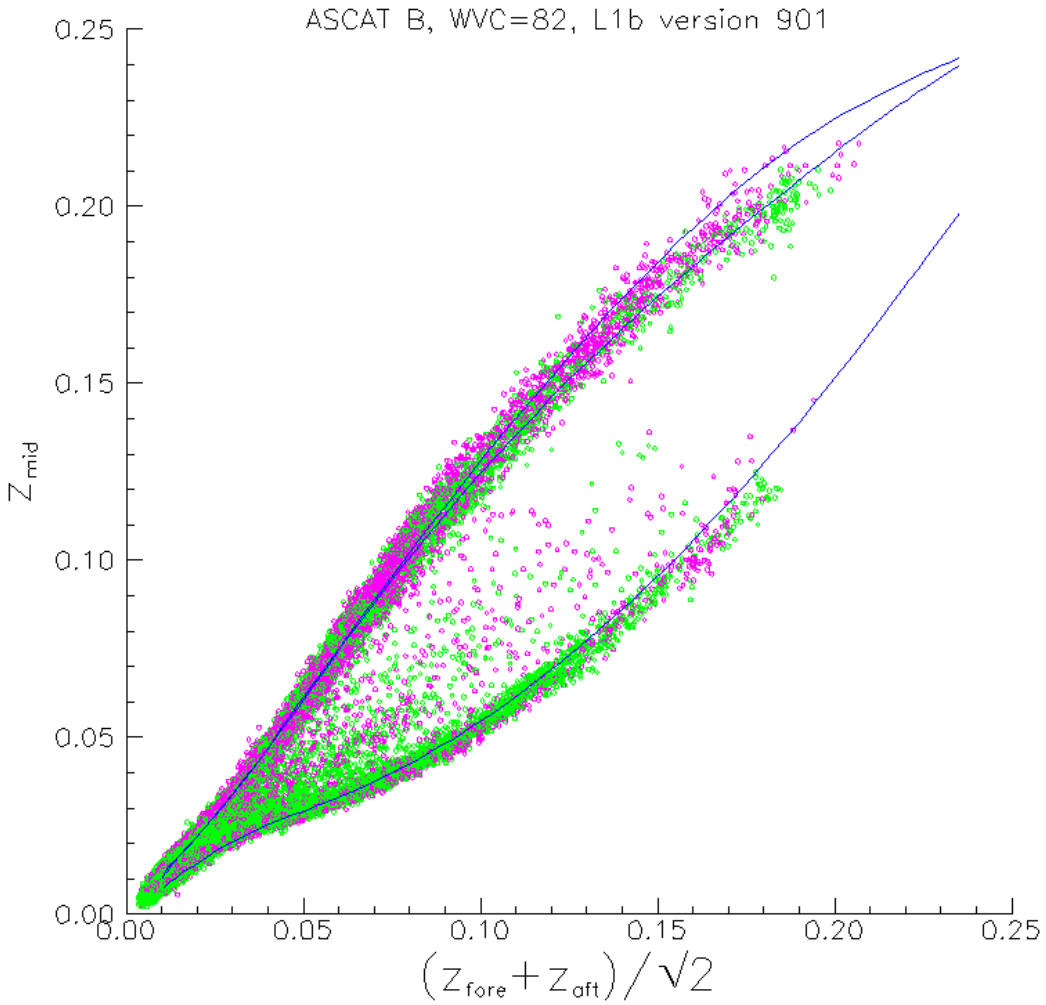

Figure 7 - Projection of the CMOD5.N wind cone (blue) and data points on the plane $z_{fore} = z_{aft.}$. Purple points belong to the upwind (outer) manifold, green points to the downwind (inner) manifold. For black points the inversion failed. Data is from L1b version 901, NOC corrected.

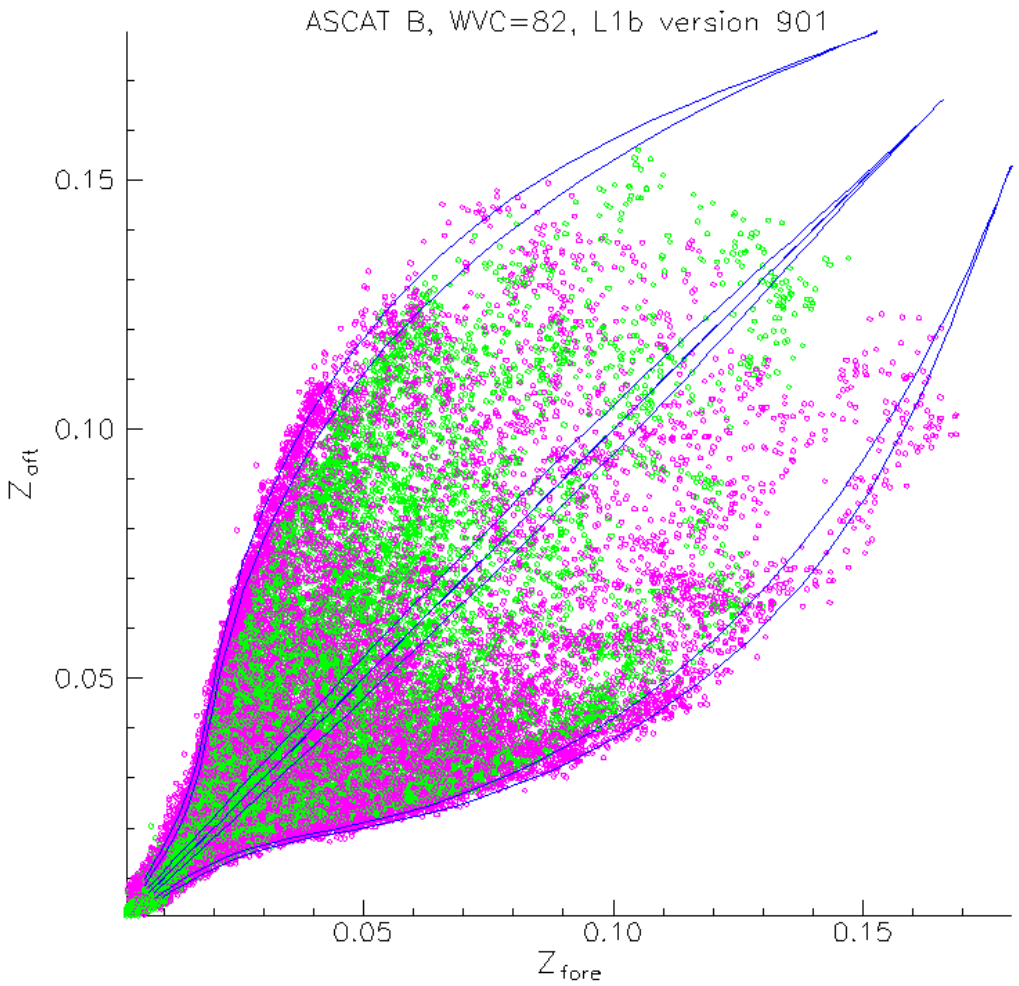

Figure 8- Projection of the CMOD5.N wind cone (blue) and data points on the plane $z_{mid} = 0$. Purple points belong to the upwind (outer) manifold, green points to the downwind (inner) manifold. For black points the inversion failed. Data is from L1b version 901, NOC corrected.

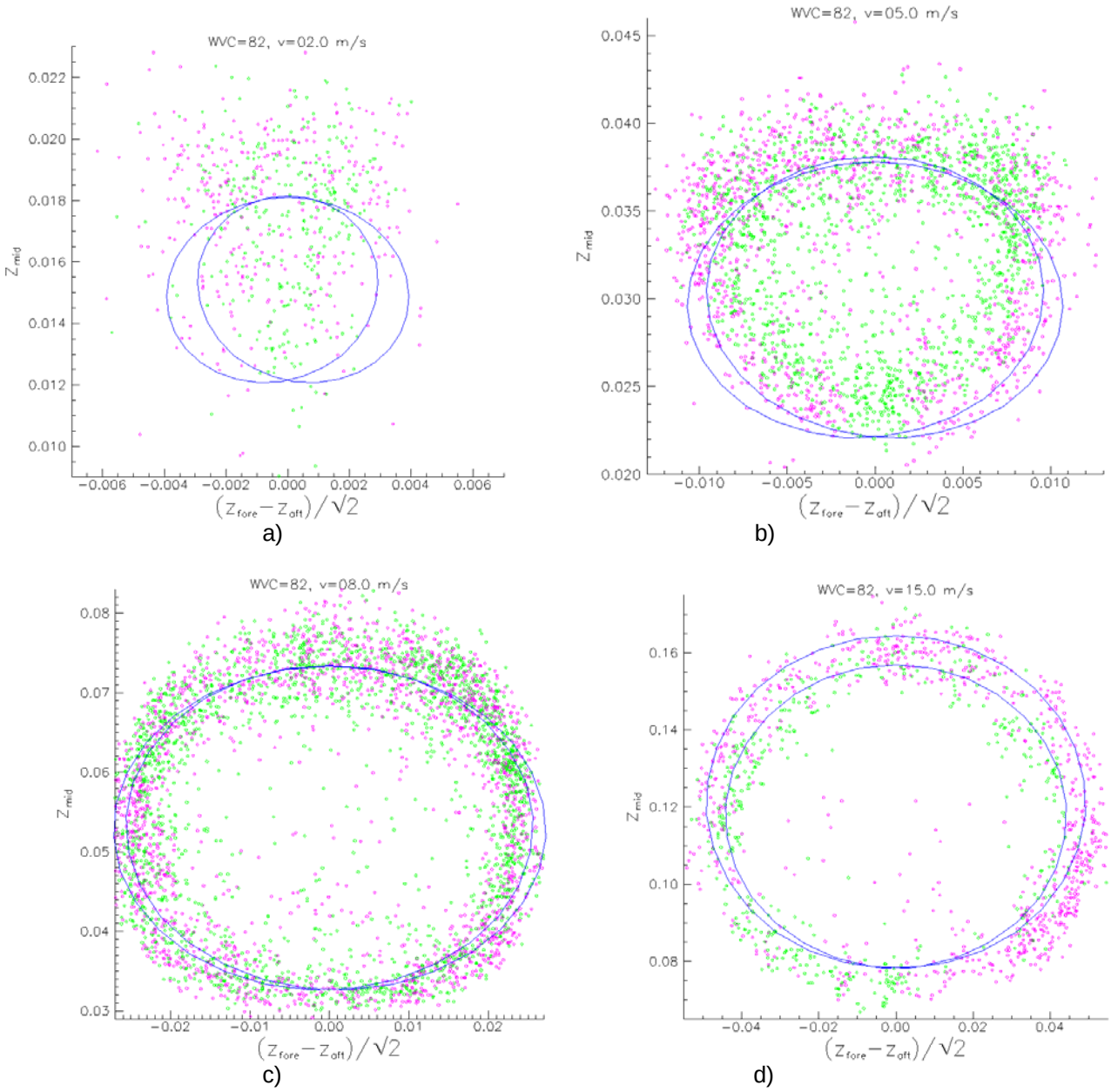

Figure 9 – Visualisation for WVC 82 of the corrected σ^0 triplets (L1b version 901) and CMOD5.N (blue ellipses), for several intersections of the cone with a slice at $z_{fore} + z_{aft} = 2z_{ref,}$. Purple points belong to the upwind (outer) manifold, green points to the downwind (inner) manifold. For black points the inversion failed. The plots correspond to the following wind speeds:
a) V = 2 m/s b) V = 5 m/s c) V = 8 m/s d) V = 15 m/s

Figure 10a) and b) show the total correction factors for the L1b version 901 and 801 respectively. The level 1b corrections from Figure 3a) has been added to the total correction factors for the level 1b version 801 data (=NOC correction) in order to generate the total correction factors for the level 1b version 901 data. The patterns look very consistent for all antennas. This is an indication that the inter-beam biases are small and that only an overall correction, which is basically incidence angle dependent is needed. For high incidence angles the correction is still large, i.e., around +0.7 dB. This is likely to be caused by a CMOD5.N issue, since CMOD5.N has not yet been validated for such high incidence angles. We suggest ancillary sea ice, rain forest and soil geophysical comparisons to gain confidence in the backscatter calibration in the outer swath.

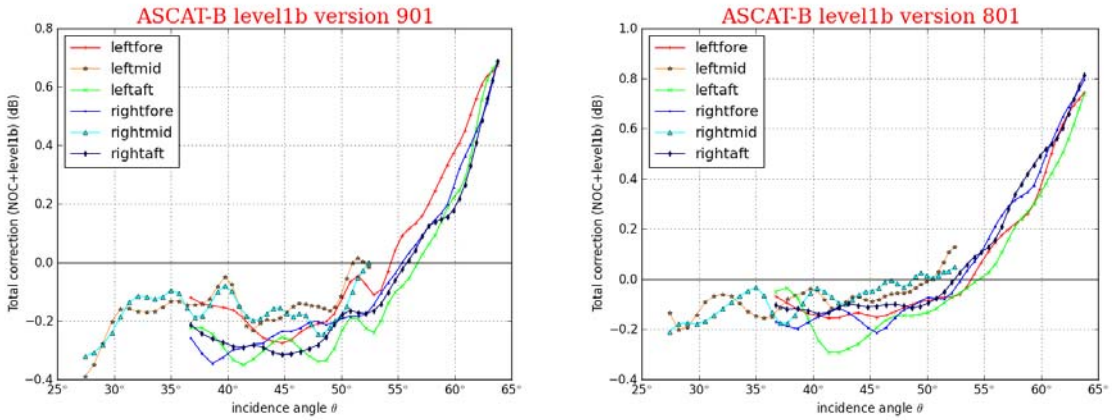

a) b)

Figure 10 – Total correction factors (NOC+L1b) per antenna and incidence angle
a) L1b version 901 data
b) L1b version 801 data

The tables with total correction factors can be found in and applied with awdp_prepost.F90 subroutine calibrate_s0.
The tables with the individual NOC and L1b correction factors can be found in awdp_tables.F90 and applied with subroutines correct_NOC and correct_l1b respectively.

6 NWP backscatter comparison

A NWP simulated backscatter comparison [Verspeek 2006] is performed with the parallel L1b version 901 and 801 data steams, both with total correction factors applied. Both L1b products are processed with AWDP using 2D-VAR ambiguity removal to provide a level 2 product with scatterometer retrieved winds and collocated NWP winds from the ECWMF model. The data is conservatively filtered to exclude land and ice. The residuals are the differences between the averaged measured σ^0 values and the averaged σ^0 values simulated from the NWP winds.

Figure 11 shows the ocean calibration residuals with the use of the CMOD5na GMF. CMOD5na is identical to CMOD5n with the addition of a 3rd order polynomial fit function to the total correction factors of ASCAT-A. This GMF is described in more detail in [Verspeek 2012]. Both ASCAT-B level 1b versions 801 and 901 show wiggles. The version 901 residuals are closer to zero and thus more in agreement with ASCAT-A.

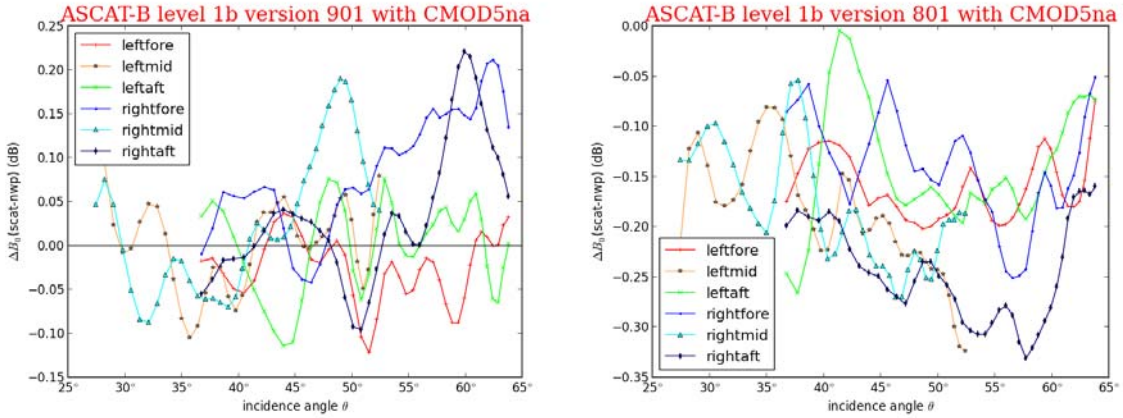

Figure 11 – Ocean calibration residuals for CMOD5na per antenna and incidence angle
a) L1b version 901 data
b) L1b version 801 data

Figure 12 shows the results of an oceancalibration with CMOD5n where also the level 1b corrections have been applied. The difference ranges from -0.20 dB to +0.06 dB. This is a clear improvement with respect to the uncorrected cases (see Figure 10). The difference between Figure 12a) and Figure 12b) is very small. The L1b corrections have effectively made the results alike.

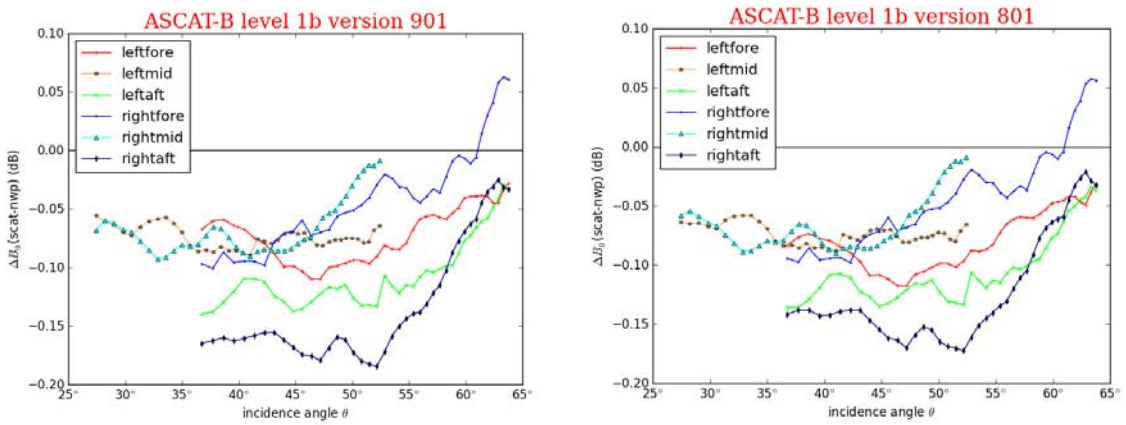

a) b)

Figure 12 – Ocean calibration residuals of ASCAT backscatter values and simulated backscatter values from ECMWF real 10m winds. Data is from 2013-05-30 to 2013-06-03.
a) L1b version 901 with CMOD5n+NOC+level 1b corrections
b) L1b version 801 with CMOD5n+NOC+level 1b corrections

7 Wind statistics

In this section some statistics plots comparing ASCAT wind and ECMWF wind are given. Figure 13 shows the results for both L1b version 901 and 801. The statistics for the two data sets are almost identical. This is to be expected because the L1b 901-to-801 correction is small and almost linear. The ECMWF winds are increased by 0.2 m/s in order to account for the difference between real 10-m winds (ECMWF) and equivalent neutral winds (ASCAT). When the wind speed difference shown in Figure 13a) is averaged over all WVCs it has a value of around -0.1 m/s. Figure 13b) shows the SD of the wind speed difference. Figure 13c) and Figure 13d) show the wind direction difference and SD of the wind direction difference respectively.

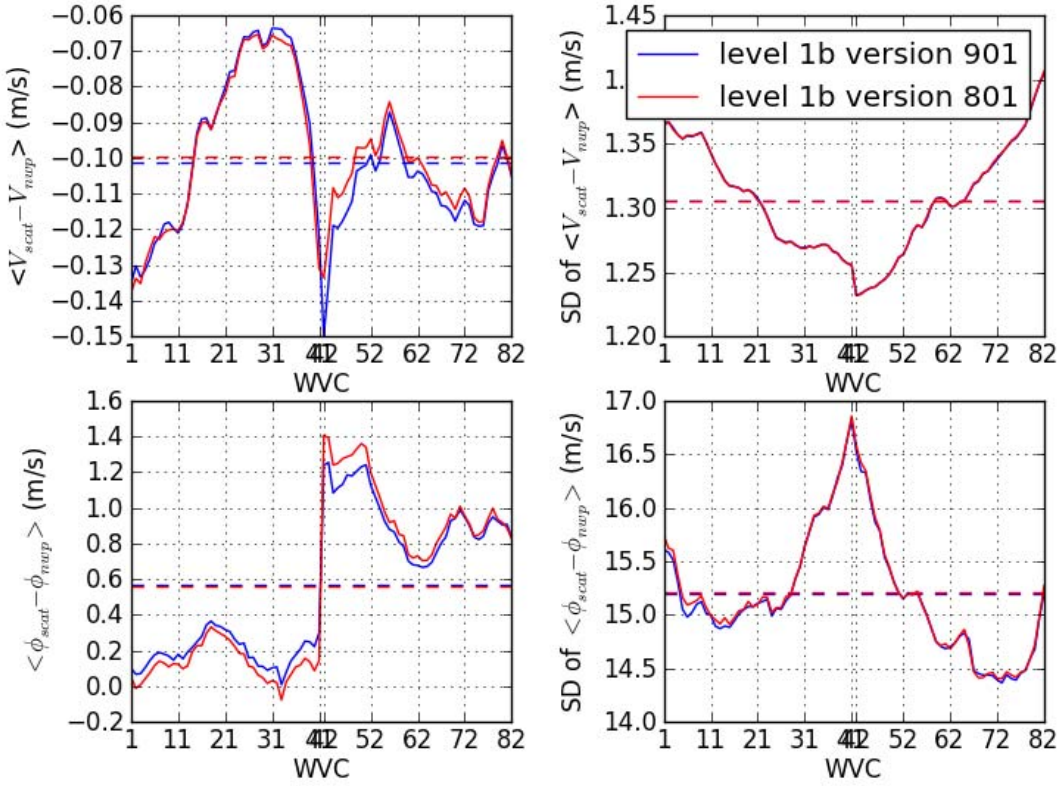

Figure 13 – Wind comparison per WVC between ASCAT and ECMWF for L1b software versions 901 and 801. Backscatter data is NOC and L1b-change corrected. Wind direction statistics are for the 2DVAR wind solutions for ECMWF U10N winds larger than 4 m/s.
upper left: average wind speed difference; upper right: wind speed SD
lower left: average wind direction difference; upper right: wind direction SD.

Figure 14 shows the wind scatter plots for L1b version 901 corrected data. L1b version 801 wind scatter plots and statistics are very similar.

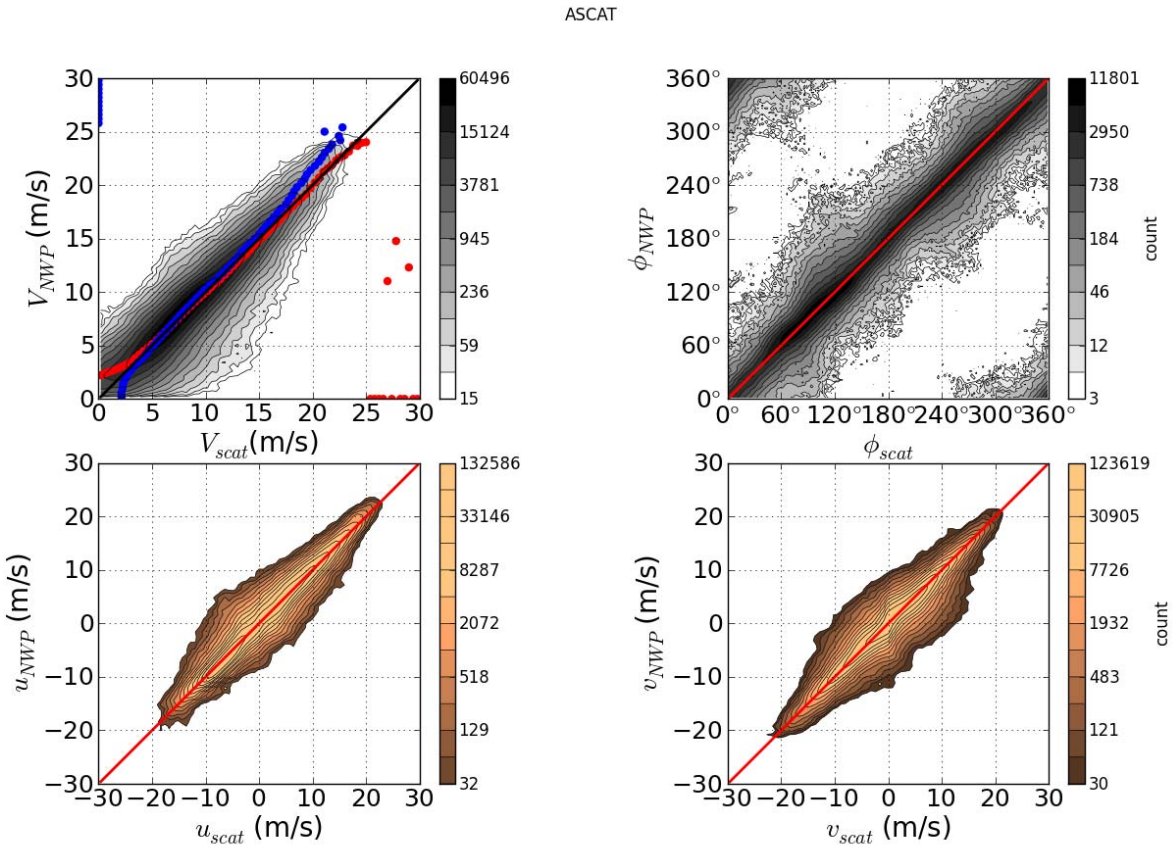

Figure 14 – Two-dimensional histogram of the 2D-VAR KNMI-retrieved wind solution versus ECMWF wind for all WVCs. The L1b version 901 data with NOC correction and L1b-change correction is used.
Upper left: wind speed (bins of 0.4 m/s). The red dots show <Vnwp> for each Vscat bin, the blue dots show <Vscat> for each Vnwp bin
Upper right: wind direction (bins of 2.5°) for ECMWF winds larger than 4 m/s.
Lower left: wind component u (bins of 0.4 m/s)
Lower right: wind component v (bins of 0.4 m/s)

7.1 Collocated wind statistics

A collocated data set is retrieved which can be used for wind statistics. The data set is obtained by taking a WVC from the L1b version 801 input and searching the L1b version 901 input stream for the WVC with the closest distance to the version 801 WVC. The search is restricted to a limited time frame in which the collocation is to be expected. Also the WVC numbers must match. Thus for every input "801" WVC a matching "901" WVC can be found. Apart from the collocation critera other filter criteria can be applied to each input stream.

Figure 15 shows the scatterometer wind speed and wind direction for the two L1b versions. Both streams are highly correlated. They are constructed from the same full-resolution data and are collocated. The high correlation is also reflected in the small values of the SD for the difference in wind speed and wind direction, 0.045 m/s and 1.81^{o} respectively.

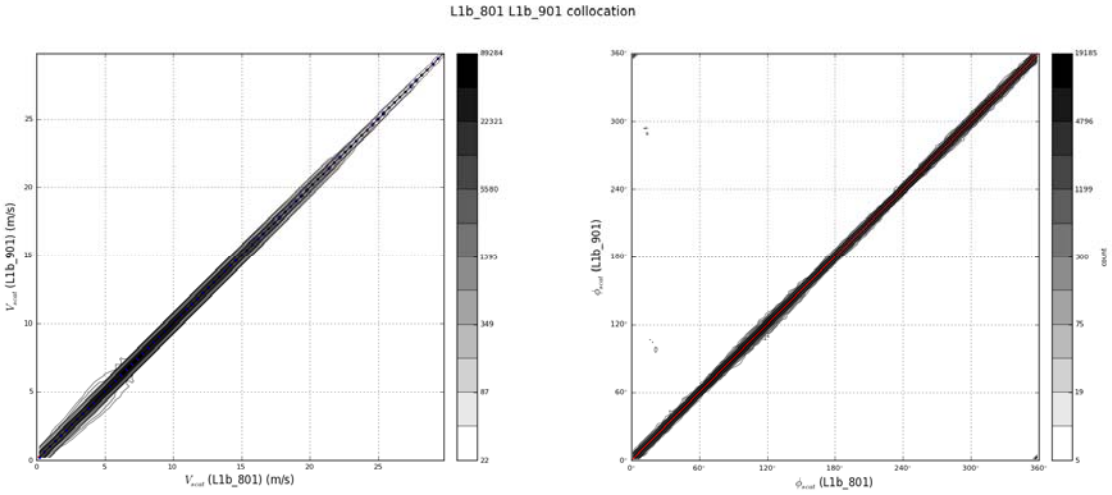

Figure 15 – Two-dimensional histograms for Level 1b version 801 (horizontal axis) versus Level 1b version 901 (vertical axis). The red dots show < (L1b 901)> for each (L1b 801) bin, the blue dots show < (L1b 801)> for each (L1b 901) bin. Bin size is 0.4 m/s and 2.5^0 for scatterometer wind speed (left) and wind direction (right) respectively. Data is from 2013-05-30.

8 MLE statistics and QC

Figure 16 shows the normalised distance to cone or Maximum Likelihood Estimator (MLE) [Portabella and Stoffelen 2006] as a function of WVC for L1b version 901 corrected data. The data range is divided into 15 levels equally spaced on a logarithmic scale, each successive level is a factor of two higher than the previous level. For low MLE values there is no dependency on WVC number. For higher MLE values a dependency on WVC number can be seen that is symmetric for the left and right swath, so in fact the dependency is on mid beam incidence angle. The plot for L1b version 801 data is very similar.

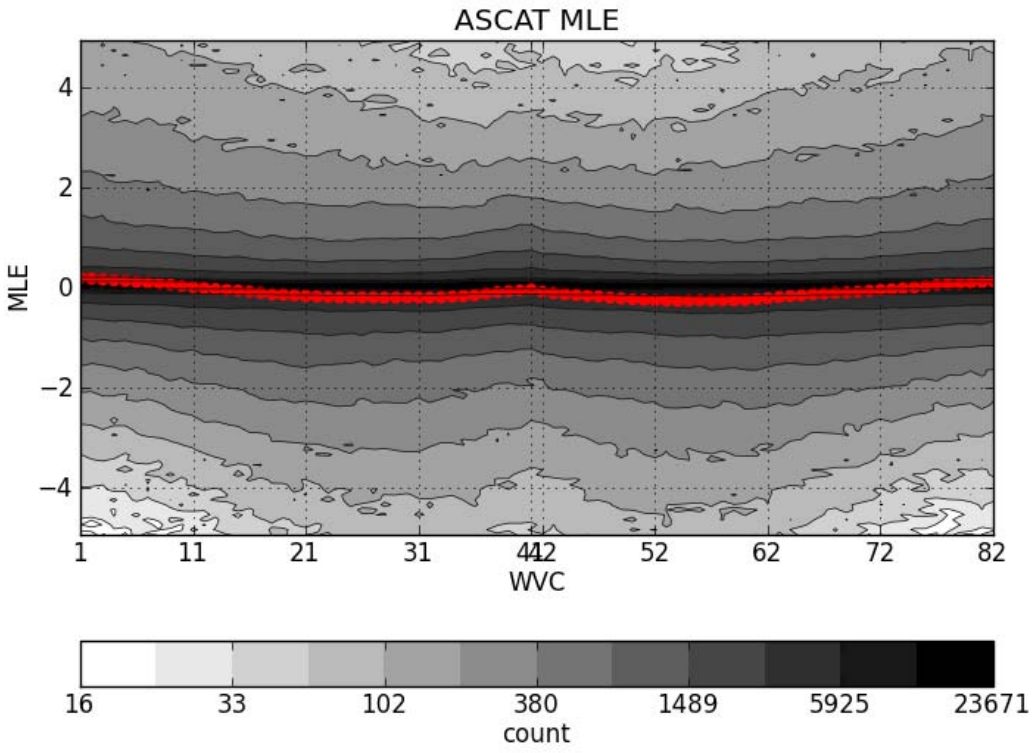

Figure 16 - MLE distribution per WVC shown for L1b version 901 corrected data. The data range is divided into 15 levels equally spaced on a logarithmic scale, each successive level is a factor of 2 higher than the previous level.

Figure 17 shows the MLE as a function of the scatterometer wind speed for L1b version 901 corrected data. For high wind speed values the cone cross section is large compared to the spread of the triplets around the cone surface. A symmetrical pattern around the origin is expected here as an equal amount of triplets are on the inner and outer side of the cone surface (see Figure 9). For low wind speed values, i.e., smaller than ~4 m/s, the cone radius is small and the spread of triplets is relatively large. More triplets are expected to lie outside the cone and thus have a negative MLE.

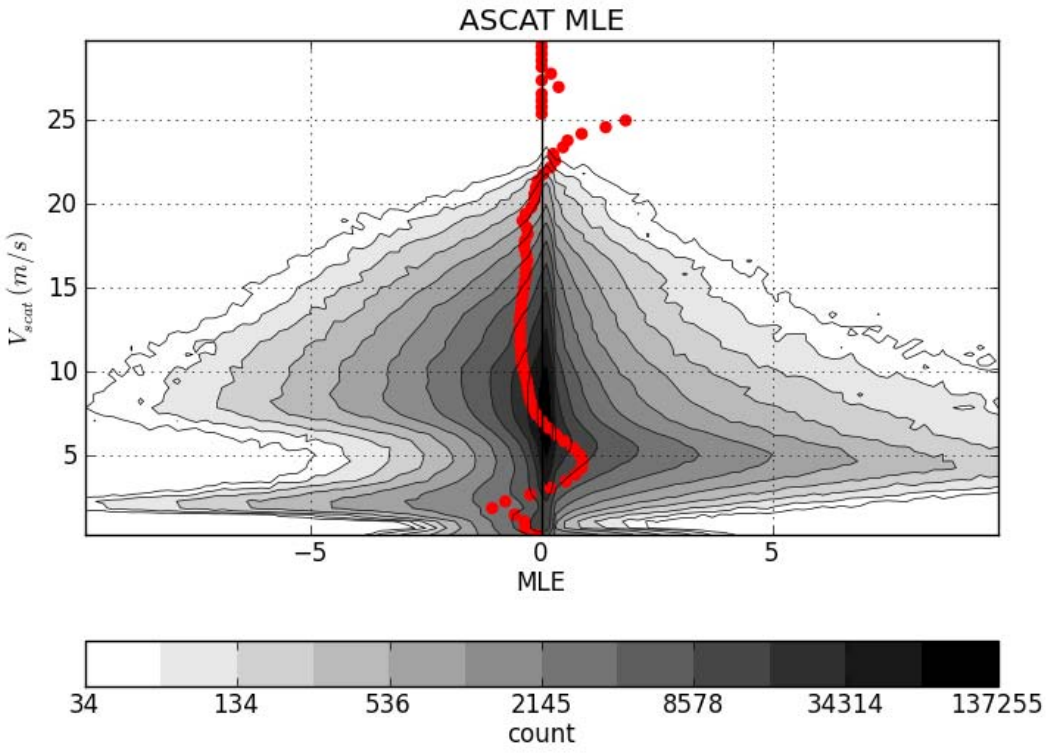

Figure 17 – Cone distance distribution versus measured wind speed for corrected L1b version 901 data. In red the average MLE values are shown.

Note that around 5 m/s most corrected triplets lie within the cone. This corresponds to earlier assessments that the CMOD5.N cone is too wide for these winds [Portabella and Stoffelen, 2006]. After the ASCAT Cal/Val, we anticipate to use the MLE to correct CMOD5.N.

In Figure 18 the contourplot of the MLE for L1b version 801 and 901 is shown for the collocated set. They show a high correlation (R=0.0992) indicating close performance for the two versions.

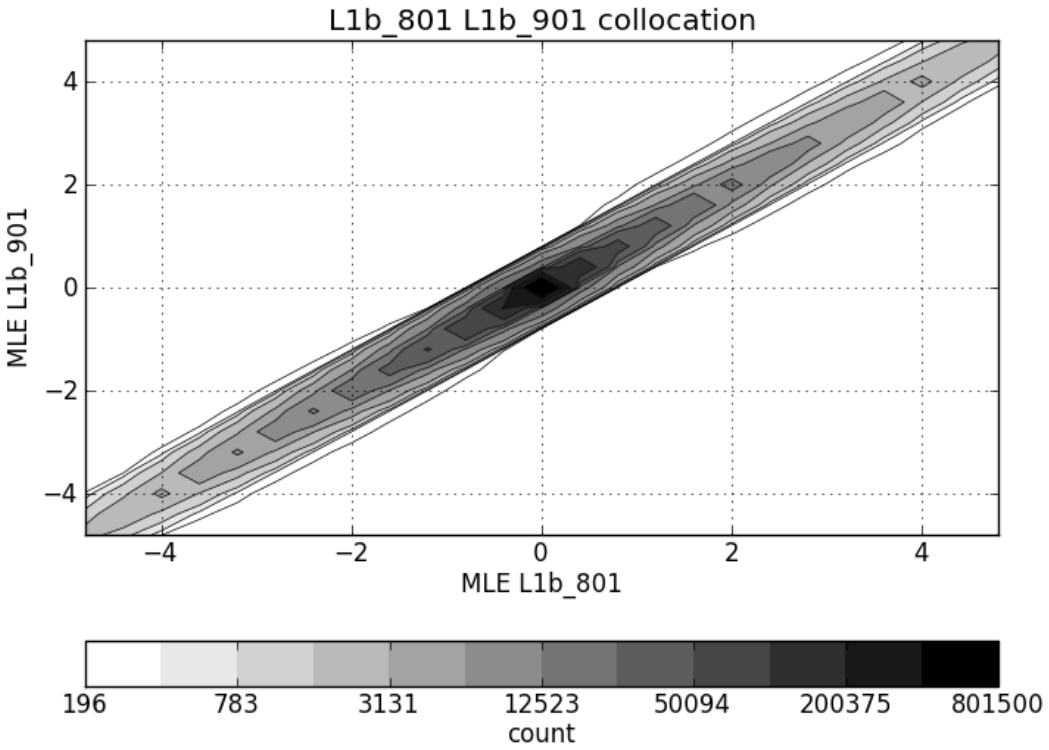

Figure 18 – Cone distance histogram for Level 1b version 801 (horizontal axis) versus Level 1b version 901 (vertical axis). Data is from 2013-05-30.

The MLE or GMF distance flag is set when the measured triplet has an anomalously large distance to the GMF cone, while the var_qc flag is set during 2DVAR ambiguity removal when a wind vector is spatially inconsistent with its neighbours. The knmi_qc flag is a collection flag that comprises the GMF, kp and ice flag. Figure 19 shows some level 2 quality flag occurrences as a function of WVC number. Figure 19a) and b) show the 12.5 km resolution of L1b version 901 and 801 respectively.

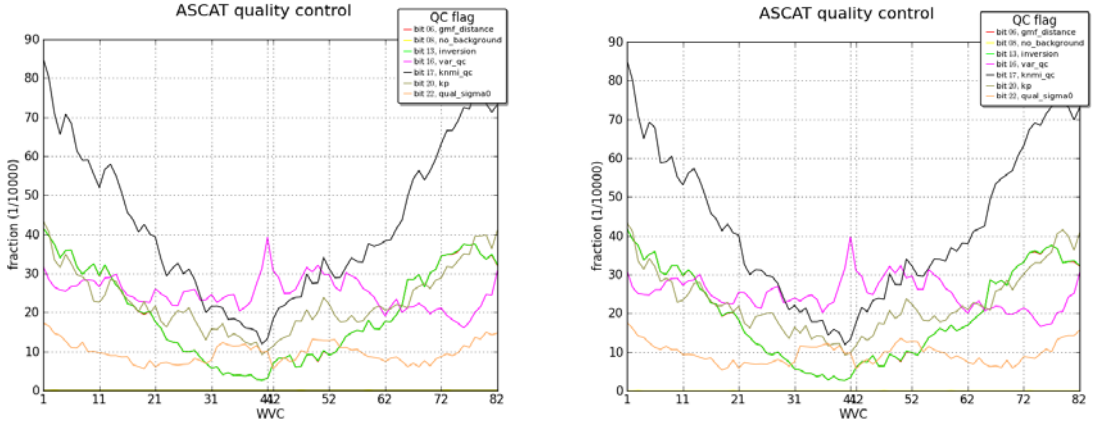

a) b)

Figure 19 – ASCAT quality flags occurrence as a function of WVC number. Results are shown for all wind speeds, including those below 4 m/s, L1b corrections and NOC corrections are applied.
a) 12.5 km resolution L1b version 901
b) 12.5 km resolution L1b version 801

The rejection rate increases when we go from the inner part to the outer part of the swath. This can be explained as follows. The cone opens up with incidence angle. Therefore, larger MLE values

inside the cone are more frequent in the outer swath (less aliasing effect). Also noise is somewhat lower at higher incidence angles, which reduces the MLE norm. These effects bring more data into the tail of the MLE distribution at high incidence angles and therefore increase the QC rejection rate.

In Table 1 the knmi_qc flag rejections are shown for level 1B version 801 and 901. The collocated data set from 2013-05-30 is used as in Figure 15. The number of WVCs with (801 set and 901 not set) divided by the total number of WVCs with (801 set) is 9%. The shift in geolocation between the two versions will likely contribute to this number.

knmi_qc	Total	801(set)	801(not set)
Total	1937250	4608	
901(set)	4586	4195	391
901(not set)		413	

Table 1 – Comparison of knmi_qc rejections for level 1B versions 801 and 901. Data is in 12.5 km resolution from 2013-05-30.

Routine monitoring statistics are accessible through the OSI SAF ASCAT product viewer web site: http://www.knmi.nl/scatterometer/ascat_b_osi_25_prod/ascat_app.cgi and http://www.knmi.nl/scatterometer/ascat_b_osi_co_prod/ascat_app.cgi by selecting “Monitoring information”.

9 Conclusions

The EUMETSAT transponder calibration effectively results in new ASCAT-B instrument gain values at each Wind Vector Cell (WVC) for each of the fore, mid and aft beams. In this report we describe and evaluate level 1b (L1b) corrections to the operational L1b ASCAT backscatter data version 901 (relative to 801) as provided by EUMETSAT based on their three transponder calibration campaign. Based on the OSI SAF cone visualisation tools at KNMI and the NWP Ocean Calibration (NOC) procedure, calibration of the ASCAT-B scatterometer is checked. Indeed, after reverse corrections the ASCAT wind product based on L1b version 901 shows very similar characteristics to the ASCAT scatterometer wind product based on L1b version 801 and meets the wind product requirements.

The ASCAT L1b version 901 backscatter data are compared to the currently used version 801 backscatter data. For the corrected case, consistency between the two sets is found. The level 2 monitoring statistics, like average MLE, average wind speed bias with respect to the NWP wind speed, SD of the wind speed and wind direction show almost identical pictures for both the L1b versions. When using the correction table, the level 2 wind product is of high quality.

In the outer swath consistent large departures remain for the uncorrected case. The aim is to get also a high-quality product without using a correction table. This could be easily achieved by incorporating the correction table in the CMOD fit-parameters. The current corrections may be split in a GMF dependent part, which lead to the development of CMOD5Na, and a remaining antenna-dependent part, named NOCa. Initial results for CMOD5Na+NOCa are promising and show very little difference in wind quality compared to the present CMOD5N+NOC combination. The current NOCa corrections from the ocean calibration are relevant and uncorrected (CMOD5Na) wind retrievals are not acceptable as a level 2 wind product.

This issue should be resolved by checking against other ancillary geophysical data like from sea ice or rain forest surfaces. This could be done by making the NOCa corrections available for these other products. This will help in resolving any remaining errors in, and assessing the validity of, the CMOD5Na GMF and L1b calibration, especially for the high incidence angles.

Acronyms and abbreviations

.

Name	Description
AMI	Active Microwave Instrument
ASCAT	Advanced scatterometer
AWDP	Ascat Wind Data Processor
BUFR	Binary Universal Form for Representation (of meteorological data)
CMOD	C-band geophysical model function used for ERS and ASCAT
ECMWF	European Centre for Medium-Range Weather Forecasts
ERA40	ECMWF 40 year reanalysis
ERS	European Remote sensing Satellite
ESA	European Space Agency
ESDP	ERS Scatterometer Data Processor
EUMETSAT	European Organization for the Exploitation of Meteorological Satellites
GMF	geophysical model function
KNMI	Koninklijk Nederlands Meteorologisch Instituut (Royal Netherlands Meteorological Institute)
METOP	Meteorological Operational satellite
MLE	maximum likelihood estimator (used for distance to cone)
NWP	numerical weather prediction
OSI	Ocean and Sea Ice
QC	Quality Control (inversion and ambiguity removal)
SAF	Satellite Application Facility
SD	standard deviation
WVC	wind vector cell, also known as node or cell

Table 2 - List of acronyms and abbreviations

References

[Anderson 2012] Craig Anderson, Hans Bonekamp, Julia Figa (eumetsat), Monitoring ASCAT-A Calibration using Ocean Backscatter, IOVWST 2012, Utrecht, the Netherlands.

[Figa 2004] Figa-Saldaña, Julia, "ASCAT calibration and validation plan", *EUMETSAT*, EPS programme, Darmstardt Germany, 2004

[Figa et al 2002] Figa-Saldaña, J., J.J.W. Wilson, E. Attema, R. Gelsthorpe, M.R. Drinkwater, and A. Stoffelen, The Advanced scatterometer (ASCAT) on the meteorological operational (MetOp) platform: A follow on for the European wind scatterometers, Can. J. Remote Sensing ***28*** *(3)*, pp. 404-412, 2002.

[Hersbach 2007] Hersbach, H., A. Stoffelen, and S. de Haan , An improved C-band scatterometer ocean geophysical model function: CMOD5, J. Geophys. Res., 112, C03006, 2007. See also www.knmi.nl/scatterometer/cmod5/

[Portabella and Stoffelen 2006] Marcos Portabella, Ad Stoffelen, Scatterometer backscatter uncertainty due to wind variability, IEEE Trans. Geosci. Rem. Sens. **44** (11), 3356-3362, 2006.

[Portabella and Stoffelen 2009] Portabella, M., and Stoffelen, A., "On scatterometer ocean stress," submitted to J. Atm. and Ocean Techn., 26 (2), pp. 368–382, 2009.

[Stoffelen 1999] Stoffelen, Ad, "A Simple Method for Calibration of a Scatterometer over the Ocean", J. Atm. and Ocean Techn. 16(2), 275-282, 1999.

[Stoffelen 1998] Stoffelen, Ad, "Scatterometry", KNMI*, PhD thesis at the University of Utrecht*, ISBN 90-39301708-9, October 1998

[Stoffelen and Anderson 1997] Stoffelen, Ad, and David Anderson, "Scatterometer Data Interpretation: Measurement Space and inversion", J. Atm. and Ocean Techn., 14(6), 1298-1313, 1997.

[Verhoef et al 2008] Verhoef, A., M. Portabella, A. Stoffelen and H. Hersbach, "CMOD5.n - the CMOD5 GMF for neutral winds", OSI SAF Technical Report SAF/OSI/CDOP/KNMI/TEC/TN/165, 2008

[Verspeek 2006] Verspeek, Jeroen, "Scatterometer calibration tool development", EUMETSAT Technical Report SAF/OSI/KNMI/TEC/RP/092, *KNMI*, de Bilt, 2006,

[Verspeek 2006-2] Verspeek, Jeroen, "User manual Measurement space visualisation package", *KNMI*, de Bilt, 2006

[Verspeek et al 2011] Verspeek, J., Portabella, M., Stoffelen and A. Verhoef, A, "Calibration and Validation of ASCAT Winds", EUMETSAT Technical Report SAF/OSI/KNMI/TEC/TN/163 KNMI, de Bilt, 2011

[Verspeek 2011-2] Verspeek, J. and Stoffelen, A. "ASCAT GMF", DRAFT, *KNMI*, de Bilt, 2011

[Verspeek 2012] Verspeek, J., Stoffelen, A., Verhoef, A. and Portabella, M., "Improved ASCAT Wind Retrieval Using NWP Ocean Calibration," Geoscience and Remote Sensing, IEEE Transactions on , vol.50, no.7, pp.2488,2494, July 2012

[Verspeek, Verhoef and Stoffelen 2013] Verspeek, J., Verhoef, A and Stoffelen, ASCAT-B NWP Ocean Calibration and Validation, EUMETSAT Technical Report SAF/OSI/CDOP2/KNMI/TEC/RP/199, KNMI, de Bilt, 2013

[Vogelzang et al. 2011] Vogelzang, J., A. Stoffelen, A. Verhoef, and J. Figa-Saldaña (2011), On the quality of high-resolution scatterometer winds, J. Geophys. Res., 116, C10033, doi:10.1029/2010JC006640.